Bulletin of the Seismological Society of America, Vol. 103, No. 6, pp. –, December 2013, doi: 10.1785/0120130020

Rock and Stiff-Soil Site Amplification: Dependency on V_{S30} and Kappa (κ_0)

by A. Laurendeau, F. Cotton, O.-J. Ktenidou, L.-F. Bonilla, and F. Hollender*

Abstract A ground-motion prediction equation (GMPE) specific to rock and stiff-soil sites is derived using seismic motion recorded on high V_{S30} sites in Japan. This GMPE applies to events with $4.5 \leq M_w \leq 6.9$ and V_{S30} ranging from 500 to 1500 m/s (stiff-soil to rock sites). The empirical site coefficients obtained and the comparison with the simulated site functions show that seismic motion on rock and stiff-soil sites does not depend only on V_{S30}, but also on the high-frequency attenuation site properties (κ_0). The effects of the site-specific κ_0 on site amplification are analyzed using stochastic simulations, with the need to take into account both of these parameters for rock-site adjustments. Adding the site-specific κ_0 into the GMPEs thus appears to be essential in future work. The rock-site stochastic ground-motion simulations show that the site-specific κ_0 controls the frequency corresponding to the maximum response spectral acceleration ($f_{amp}1$). This observation is used to link the peak of the response spectral shape to κ_0 in this specific Japanese dataset and then to add the effects of high-frequency attenuation into the previous GMPE from the peak ground acceleration and up to periods of 0.2 s. The inclusion of κ_0 allows the observed bias to be corrected for the intraevent residuals and thus reduces sigma. However, this κ_0 determination is limited to a minimum number of rock-site records with $M_w \geq 4.5$ and to distances of less than 50 km.

Introduction

Defining a standard rock site is a key issue for seismic-hazard analysis. Rock properties vary from one region to another, and recent probabilistic seismic-hazard assessment projects (e.g., Seismic Hazard Harmonization in Europe) have shown the need to clearly define the reference rock used for hazard computations (e.g., Delavaud *et al.*, 2012). A reference rock is also necessary as a basis for the amplification calculations, and, for example, for the analysis of site effects by the spectral-ratio method (Borcherdt, 1970).

Indeed, definitions of "rock" conditions are highly heterogeneous and have evolved over the last few years. Before 1995, ground-motion empirical models considered a binary classification for sites as rock or soil, based on geological criteria or on the thickness of the sediments. Then, the new building codes defined site categories with respect to the average shear-wave velocity over the upper 30 m (the V_{S30}). Thus, the National Earthquake Hazard Reduction Program (NEHRP) regulations (Building Seismic Safety Council, 2000) define a rock class as a site with $V_{S30} > 760$ m/s, and a very hard rock class as a site with $V_{S30} > 1500$ m/s, while the European regulations (European Committee for Standardization [CEN], 2004) define rock sites as those with $V_{S30} > 800$ m/s, and the Japanese regulations (Japan Road Association, 1980, 1990) define rock sites as those with $V_{S30} > 600$ m/s. Ambraseys (1995) and Boore *et al.* (1997) were the first to incorporate V_{S30} into their models. Currently, many recent ground-motion prediction equations (GMPEs) include V_{S30} (e.g., Abrahamson and Silva, 2008; Boore and Atkinson, 2008; Rodriguez-Marek *et al.*, 2011). However, these models are derived by mixing soil and rock data. At the same time, the Next Generation Attenuation (NGA) and the European databases contain only a few records on high V_{S30} sites, and high quality measures of V_{S30} are not always available (e.g., Regnier *et al.*, 2010). Indeed, V_{S30} values are not always reliable, due to the uncertainties of indirect estimates, especially in the case of rigid sites for which it is difficult to apply several techniques of measurement (e.g., boreholes, standard penetration tests, multichannel analysis of surface waves). The rock-site factors of these models might suffer from this lack of data or from V_{S30} uncertainties.

Moreover, the use of V_{S30} as a single proxy to define rock conditions has been discussed widely, as V_{S30} describes only the shallow part of the velocity profile and does not capture the effects of shallow crustal attenuation. Several studies have suggested that the rock properties can control part of the high-frequency attenuation (Silva *et al.*, 1998; Chandler *et al.*, 2006; Douglas *et al.*, 2010; Edwards *et al.*, 2011). This high-frequency decay was initially described by Hanks (1982), as the cutoff frequency f_{max}. Today, for a record at distance r, the model used for high-frequency attenuation is

*Also at ISTerre, CNRS, Université Joseph Fourier, BP 53, 38041 Grenoble Cedex 9, France.

usually characterized in the engineering seismology community by the parameter kappa [$\kappa(r)$]. $\kappa(r)$ describes the slope of the high-frequency decay of the acceleration Fourier amplitude spectrum in a log–linear space (Anderson and Hough, 1984). The model is described as

$$a(f) = A_0 \exp[-\pi\kappa(r)f] \quad \text{for } f > f_E, \tag{1}$$

in which A_0 is a source- and propagation-path-dependent amplitude, f_E is the frequency above which the decay is approximately linear, and r is the epicentral distance. The distance-dependence can then be eliminated by extrapolating the $\kappa(r)$ trend to $r = 0$, introducing a site-specific kappa, typically denoted as κ_0, that is free of the regional Q attenuation effect added by distance. Anderson and Hough (1984) suggested that κ_0 represents the attenuation of seismic waves in the first few hundreds of meters or kilometers beneath the site and that it depends on the site conditions. In the literature, there are other ways to measure the site-specific κ_0 in addition to the original method of Anderson and Hough (1984). Here, in the present study, when we talk about κ_0 in general, this is kappa for a specific site; when we talk about κ_0 computed with a specific method, we add a subscript indicating that method, as recommended by Ktenidou *et al.* (2013).

Several studies have explored the relationships between geotechnical site properties (e.g., V_{S30}) and κ_0 (Silva *et al.*, 1998; Chandler *et al.*, 2006; Edwards *et al.*, 2011). Such relationships are critical, as they are the only way to take into account κ_0 adjustments when no site-specific records are available. Recently, Van Houtte *et al.* (2011) assessed κ_0 for Japanese and NGA sites, to define a worldwide logarithmic relationship between κ_0 and V_{S30}. Van Houtte *et al.* (2011) also computed amplification factors from rock sites to very hard rock sites and showed the impact of κ_0 on the resulting amplification factors. Their theoretical amplification factors indicated that at high frequencies, a hard rock site should amplify more than a softer rock site due to its lower attenuation. Atkinson and Boore (2011) reported the same tendency for the amplification factor between the rock of western North America and the hard rock of eastern North America. However, these theoretical amplification ratios have not been confirmed yet by observations. Moreover, the correlations between κ_0 and V_{S30} are weak; for example, Van Houtte *et al.* (2011) obtained a correlation coefficient of 0.39, and most studies have reported even smaller coefficients. Thus, there are many possibilities for κ_0 for different sites with the same V_{S30}. To a degree, this is expected due to the deeper nature of κ_0. Furthermore, Ktenidou *et al.* (2013) suggested additional possible reasons behind this large scatter, related to the way the correlations are developed and used. Such reasons include the variety of regions where data come from, the variety of methods applied to compute kappa and the variability due to the differences in the used frequency ranges (e.g., Douglas *et al.*, 2010).

The general goal of the present study is to better constrain the ground motion on rock. On this basis, an active Japanese shallow crustal accelerometric dataset was built that includes only surface records on sites with $V_{S30} \geq 500$ m/s. It should be noted that the usefulness of V_{S30} as a site predictor is still under debate and that even sites with rather high V_{S30} may show large impedance contrasts at shallow depth and hence strong amplification peaks at high frequencies (e.g., see Cadet *et al.*, 2010, for KiK-net data and Zhao *et al.*, 2006, for K-NET data). This V_{S30} based site classification is however consistent with building codes and GMPE site classification schemes. This limit of 500 m/s allows a sufficient number of records and soft rock to be considered (Californian rock is usually characterized by $V_{S30} = 620$ m/s; e.g., Boore and Joyner, 1997). This dataset is used to derive a "rock/stiff-soil-specific" prediction equation. In the first step, the site amplification factors depend on V_{S30}. Our analysis will focus more specifically on the site amplification analysis obtained, as rock V_{S30}-dependent amplification factors have been poorly constrained to date, due to there being few records on high V_{S30} sites. We will compare the empirical amplification factors obtained with the theoretical factors computed for various V_{S30}/κ_0 values, and we will discuss the relative dependency of rock motion on κ_0 and V_{S30}. In the second step, new amplification factors that depend both on V_{S30} and κ_0 will be derived and discussed.

The Japanese Dataset

Japan is in an area of high seismicity, where a lot of quality digital data are recorded and made available to the scientific community. Indeed, after the destructive 1995 Kobe earthquake, Japanese scientists installed dense and uniform networks that cover the whole of Japan: the Hi-net (high sensitivity), F-net (broadband), KiK-net, and K-NET (strong motion) networks (Okada *et al.*, 2004). The KiK-net network offers the advantage of combining pairs of sensors (one at the surface and one installed at depth in a borehole). Each instrument is a three-component seismograph with a 24-bit analog-to-digital converter; the KiK-net network uses 200 Hz (until 27 January 2008) and 100 Hz (since 30 October 2007) sampling frequencies, and the K-NET network uses 100 Hz sampling frequencies. The overall frequency response characteristics of the total system is flat, strictly speaking, from 0 to 15 Hz, after which the amplitude starts to decay. The response characteristics are approximately equal to those of a three-pole Butterworth filter with a cutoff frequency of 30 Hz (Kinoshita, 1998; Fujiwara *et al.*, 2004). This filter restricts the analysis to frequencies below 30 Hz if the signal is not deconvolved by the transfer function (Oth, Parolai, and Bindi, 2011), if allowance is made for the 3 dB drop. In the present study, the KiK-net and K-NET strong-motion records were collected up to the end of 2009. To have consistent meta-parameters, we only used events that were characterized in the F-net catalog. Thus, the values of M_w, the hypocenter location (latitude, longitude, depth), and the rake angle that were used for the focal mechanism characterization were determined by F-net. We fixed 4.5 M_w as the low-magnitude limit of our

Table 1
Events for Which the Source Geometry is Taken into Account to Define the Source–Receiver Distance (R_{RUP})

Name	Date (yyyy/mm/dd hh:mm)	M_w	Strike (°)	Dip (°)	Length (km)	Width (km)	Reference
Kagoshima 1	1997/03/26 17:31	6.10	280	90	15	10	Horikawa (2001)
Kagoshima 2	1997/05/13 14:38	6.00	(280, 190)	(90, 90)	(9, 8)	(10, 10)	Horikawa (2001)
Yamaguchi	1997/06/25 18:50	5.90	235	86	16	12	Ide (1999)
Iwate	1998/09/03 16:58	5.70	216	41	10	10	Nakahara *et al.* (2002)
Tottori	2000/10/06 13:30	6.60	145	90	28	17.6	Ikeda *et al.* (2002)
Miyagi-Ken	2003/07/26 07:13	6.10	203	50	12	9.6	Miura *et al.* (2004)
Chuetsu	2004/10/23 17:56	6.60	216	53	24	16	Hikima and Koketsu (2005)
	2004/10/23 18:03	5.90	20	34	8	8	
	2004/10/23 18:12	5.70	20	58	8	8.3	
	2004/10/23 18:34	6.30	216	55	20	12	
	2004/10/27 10:40	5.80	39	29	8	8	
Rumoi	2004/12/14 14:56	5.70	15	25	10	10	Maeda and Sasatani (2009)
Fukuoka	2005/03/20 10:53	6.60	123	87.7	32	28	Kobayashi *et al.* (2006)
Noto-Hanto	2007/03/25 09:42	6.70	58	66	30	18	Momiyama *et al.* (2009)
Chuetsu-Oki	2007/07/16 10:13	6.70	34	36	32	24	Miyake *et al.* (2010)
Iwate-Miyagi	2008/06/14 08:43	6.90	203	37	42	18	Yokota *et al.* (2009)

The Kagoshima 2 event has been described as two fault planes. In this case, the source–receiver distances were calculated for these two planes, and the shorter distance was selected.

selection; and, to select stations located on the hardest sites, we included in the analysis only the stations with V_{S30} greater than 500 m/s. The two networks were deployed in two different geomorphological contexts: the K-NET stations were mainly constructed on sedimentary sites, and the KiK-net stations are on weathered rock or on thinner sediment sites (Okada *et al.*, 2004). Thus, on average, the site conditions of KiK-net are harder than those of K-NET (Aoi *et al.*, 2004). One advantage of the Japanese network is that the site characterization was performed homogeneously (downhole measures). The only difference is that for the K-NET network, the drilling did not reach 30 m. Thus, in the case of the KiK-net network, with the sites characterized by velocity profiles ranging from 30 to 2008 m, V_{S30} can be computed. For the K-NET network, as the surveys were made down to 20 m in depth, the V_{S30} must be estimated. Using the KiK-net velocity models, Boore *et al.* (2011) provided equations that related V_{S30} to V_{SZ} for Z ranging from 5 to 29 m, in 1 m increments. V_{S30} was thus estimated from these equations for the K-NET network. To include only crustal events, shallow events with a focal depth less than 25 km were selected. Offshore events were excluded, but we chose to include the events with $M_w \geq 5.5$ in the sea of Japan. A magnitude–distance filter was applied according to the Kanno *et al.* (2006) GMPE, which allows the bias due to untriggered stations to be eliminated (this bias could introduce an overestimation of predicted ground motions at large distances, see Fukushima and Tanaka, 1990; Fukushima, 1997). We chose 2.5 cm/s^2 as the peak ground acceleration (PGA) threshold (sensor threshold levels of 0.2 and 2 cm/s^2 for the KiK-net downhole and K-NET, respectively). All the records are corrected for baseline trends (the mean and the linear trend are removed). Following a visual inspection, faulty records (like *S*-wave triggers) and records from multi-events were eliminated or shortened. This *S*-wave trigger criterion mainly excludes data from small earthquakes at large distances (scenarios for which a large number of excellent and complete records are available); thus it does not cause any significant loss of data. A Tukey-windowing taper is applied on the last 2 s records and zeros are added to the end of the records in order to get homogeneous time-history durations. At the same time, we collected all of the fault-plane models for earthquakes with $M_w \geq 5.7$, as listed in Table 1. The source distance is the closest distance from a fault plane to the observation site, and it is the hypocentral distance in the case of earthquakes with lower magnitudes. Our dataset finally consists of 2357 three-component records for $M_w \geq 4.5$. Figure 1 shows the locations of the 405 observation sites (240 from KiK-net and 165 from K-NET) and the 132 earthquake epicenters. The magnitude–distance distribution is shown in Figure 2. Only a few of the records are still available in the near field. Figure 3 shows the V_{S30} distribution of the KiK-net and K-NET networks and, for comparison, one of the NGA (Chiou *et al.*, 2008) and European (Yenier *et al.*, 2010) databases. Our Japanese dataset contains nearly four times more records with V_{S30} greater than 500 m/s than the NGA dataset, and approximately six times more than the European database. Our dataset allows the sites with $500 \geq V_{S30} \geq 1500$ m/s to be better constrained, on the one hand, due to a more consistent number of records, and on the other because of the quality of the site characterization. However, only a few records are available on hard rock ($V_{S30} \geq 1500$ m/s).

The New Rock- and Stiff-Soil-Specific Response Spectral Acceleration Ground-Motion Prediction Equation

Many studies have been conducted to predict the response spectral accelerations for active shallow crustal regions. All of these studies have used an empirical relationship, by mixing

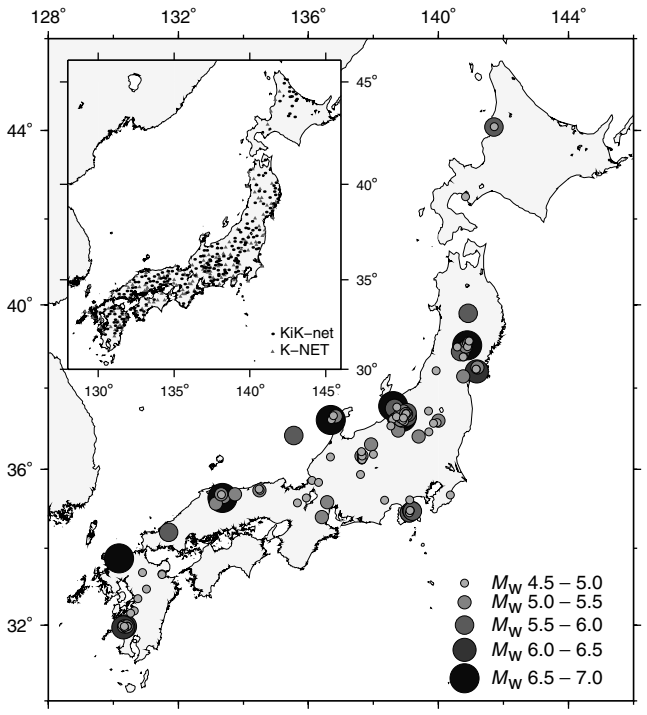

Figure 1. Events and recording stations used in the present study.

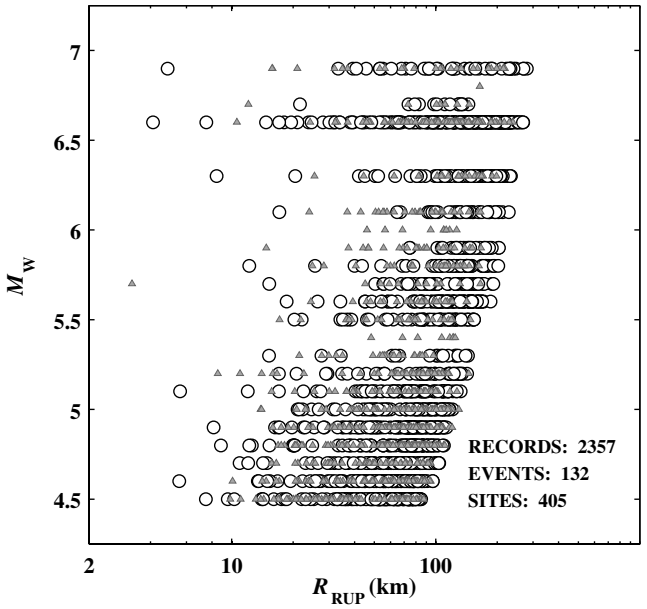

Figure 2. Distribution of the moment magnitude (M_w) and the rupture distance (R_{RUP}) of the selected records, differentiated according to the two networks (circles, KiK-net; triangles, K-NET networks).

different site classes. Moreover, these models were derived from NGA (e.g., Abrahamson and Silva, 2008; Boore and Atkinson, 2008) or European (e.g., Akkar and Bommer, 2010) databases that incorporate few data on rock, and high quality measures of V_{S30} are not always available. Only the Japanese

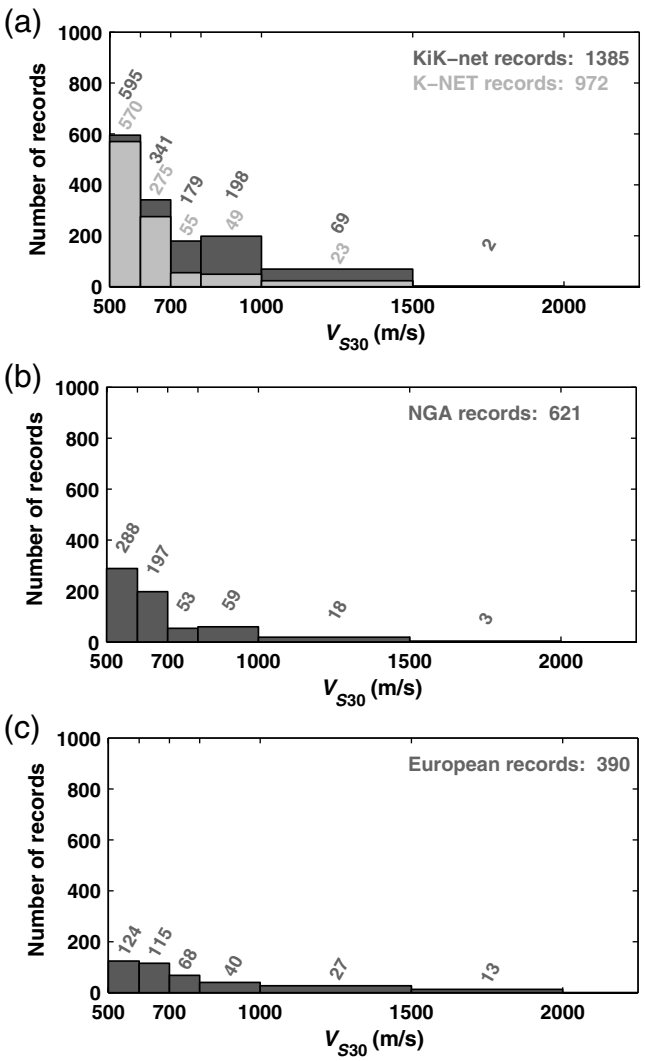

Figure 3. V_{S30} distribution in terms of the number of records: (a) for the Japanese dataset differentiated according to the two networks; and (b) and (c) for the NGA (Chiou *et al.*, 2008) and European dataset (Yenier *et al.*, 2010), respectively.

dataset offers the possibility to obtain a high-V_{S30}-specific model. A new rock- and stiff-soil-specific response spectral acceleration model from the Japanese data for the geometric mean of the two horizontal components was defined.

Model Formulation

First, all of the records are resampled to 100 Hz, to standardize the difference of sampling frequencies between K-NET and KiK-net (low-pass filter with a cutoff frequency of 100 Hz and then downsample from 200 to 100 Hz). Then, the ground-motion parameters are modeled as functions of the moment magnitude M_w, the closest distance from a fault plane to the observation site R_{RUP}, and a site parameter defined according to V_{S30}. In the present study, the aim was not to develop a new functional form, but to analyze the rock-and-stiff-soil-site amplification function. The coefficients

are derived using the random effect method of Abrahamson and Youngs (1992), taking into account the within-event (ϕ) and between-event (τ) standard deviations (Al Atik *et al.*, 2010) of the δW_{ij} and δB_i residuals, respectively (the subscripts i and j refer to event and station).

Following Rodriguez-Marek *et al.* (2011) choices, we selected a similar functional form, such as

$$\ln(\mathrm{SA}_{ij}) = F_{M_i} + F_{D_{ij}} + F_{S_j} + \delta W_{ij} + \delta B_i, \quad (2)$$

in which

$$F_{M_i} = \begin{cases} a_1 + a_2(M_{\mathrm{w}_i} - M_h) + a_3(M_{\mathrm{w}_i} - M_h)^2 & \text{for } M_{\mathrm{w}_i} \le M_h \\ a_1 + a_4(M_{\mathrm{w}_i} - M_h) & \text{for } M_{\mathrm{w}_i} \ge M_h \end{cases}, \quad (3)$$

$$F_{D_{ij}} = [b_1 + b_2(M_{\mathrm{w}_i} - 4.5)]\ln(R_{ij}/1) + b_3(R_{ij} - 1),$$
$$R_{ij} = \sqrt{R^2_{\mathrm{RUP}_{ij}} + h^2}, \quad (4)$$

$$F_{S_j} = c_1 \ln(V_{S30_j}/800). \quad (5)$$

Some of the GMPE parameters are interdependent. Therefore, some of them were constrained, starting from subsets of data. To derive GMPE coefficients from our Japanese dataset with only $V_{S30} \ge 500$ m/s was not straightforward, because the number of records per event is more limited. So, we chose to use the coefficients M_h, h, and b_3 previously derived by Rodriguez-Marek *et al.* (2011) using only events for which more than 100 records are available. Thus, we assume these parameters are not dependent on site amplification. The choice of using these coefficients comes from that they allowed us to obtain a better distribution of residuals at different spectral periods.

Results

The regression coefficients obtained are given in Table 2. Figure 4 shows the new model with respect to the three spectral accelerations: SA to (a) 0.01 s, (b) 0.31 s, and (c) 1.36 s. Figure 5 shows the interevent and intraevent residuals according to M_{w}, R_{RUP}, and V_{S30}. The residuals are well distributed globally. The model might slightly underestimate the observed data for $V_{S30} \ge 1300$ m/s at short periods, but these are few.

Our results show a standard deviation of 0.846 for the PGA while Boore and Atkinson (2008) reported a σ of 0.566 on NGA data, and Rodriguez-Marek *et al.* (2011) reported a σ of 0.799 on Japanese data. It was already recognized that the ergodic variability of ground motion is stronger for Japan (Rodriguez-Marek *et al.*, 2011), because of the larger site variability. Compared to Rodriguez-Marek *et al.* (2011), our sigma is slightly higher because our model was derived from both KiK-net and K-NET data, not just from the KiK-net data. As discussed above, the two networks were deployed in two different geomorphological contexts, which can explain this slight increase.

Rock and Stiff-Soil Ground-Motion Dependency on V_{S30} and κ_0

Comparison of Different GMPEs Dependent Only on V_{S30}

The specificity of our study is that it uses only data recorded on high V_{S30} sites ($V_{S30} \ge 500$ m/s). Figure 6 shows a comparison of our study with two other Japanese studies (Kanno *et al.*, 2006; Rodriguez-Marek *et al.*, 2011) and two NGA models (Abrahamson and Silva, 2008; Boore and Atkinson, 2008). The European models published to date do not include V_{S30} (e.g., Akkar and Bommer, 2010). These four particular studies mixed soil and rock data and included fewer records with $V_{S30} \ge 500$ m/s. To compare these site functions, we computed the ratios between soft rock and rock with V_{S30} of 550 and 1100 m/s, respectively (see Fig. 3). Our empirically derived amplification ratio is given by the following equation:

$$\frac{\text{Soft rock (550 m/s)}}{\text{Rock (1100 m/s)}}(T) = \exp\left[c_1(T)\ln\left(\frac{550}{1100}\right)\right]. \quad (6)$$

The empirical soft-rock-to-rock ratios have a similar shape globally, as a step function (see Fig. 6), with a decrease from the PGA to 0.1 s, then an increase up to different periods, and finally, at the longer periods, a plateau or a decrease. Our soft-rock-to-rock amplification ratio is lower at short periods and especially between about 0.04 and 0.08 s, for which the ratio is around 1. This suggests that the amplification of the soft rock and the rock are similar. Other models have a flatter shape at these frequencies. This slight discrepancy might be due either to the mixing of soil and rock data or to the constraints in the empirical models. Conversely, at longer periods, such as between 0.15 and 2 s, our soft rock amplifies at least 1.5 times more than rock, with a maximum at around 0.25 s.

Empirical Versus Simulated Site Function: Relative Dependencies on V_{S30} and κ_0

Atkinson and Boore (2011) and Van Houtte *et al.* (2011) observed a similar step function in the case of their theoretical rock-to-hard-rock ratio, which was dependent on both V_{S30} and κ_0. To analyze the rock ground-motion dependencies, we computed the theoretical ratios between a soft rock with $V_{S30} = 550$ m/s and a rock with $V_{S30} = 1100$ m/s. The method used to compute the theoretical ratios is synthesized in a flow chart (Fig. 7). These theoretical amplification ratios

Table 2

Regression Coefficients for the PGA and 5% Damped Acceleration Response Spectra (Geometrical Mean of the Two Horizontal Components, g)

Period (s)	a_1	a_2	a_3	a_4	M_h	b_1	b_2	b_3	h	c_1	ϕ	τ	σ
0.01	−0.033598	0.49784	−0.14873	0.22496	5.6	−0.96495	0.20938	−0.014	1.36	−0.34393	0.65621	0.53412	0.84611
0.02	−0.0050271	0.49369	−0.15747	0.23234	5.6	−0.96643	0.2069	−0.014	1.36	−0.32015	0.65584	0.53633	0.84722
0.03	0.26534	0.55346	−0.14583	0.28873	5.6	−0.98508	0.19059	−0.014	1.2	−0.19402	0.66001	0.54787	0.85777
0.0384	0.60021	0.55291	−0.21274	0.3761	5.6	−1.0008	0.16562	−0.014	1.2	−0.10368	0.67122	0.56221	0.87557
0.0484	0.86406	0.61383	−0.23459	0.48655	5.6	−0.98973	0.13542	−0.014	1.2	−0.081946	0.68807	0.57246	0.89506
0.0582	1.0014	0.83224	−0.16439	0.66501	5.6	−0.93227	0.091227	−0.014	1.2	−0.085649	0.70746	0.57719	0.91305
0.0769	1.1532	1.1502	−0.050098	0.82494	5.6	−0.85899	0.050907	−0.014	1.2	−0.074231	0.75539	0.57436	0.94895
0.0844	1.1127	1.0719	−0.10018	0.78556	5.6	−0.85513	0.060092	−0.014	1.2	−0.16829	0.76552	0.57014	0.9545
0.097	1.0339	1.083	−0.10676	0.83105	5.6	−0.84474	0.061657	−0.014	1.2	−0.31828	0.75874	0.56349	0.9451
0.1167	0.9384	1.1038	−0.042917	0.7206	5.6	−0.86975	0.09148	−0.0138	1.2	−0.46165	0.72934	0.54776	0.91213
0.1472	0.93927	0.96259	−0.078164	0.55294	5.6	−0.95779	0.13559	−0.0131	1.2	−0.64209	0.73375	0.53244	0.90658
0.1691	0.82411	0.6804	−0.22472	0.39611	5.6	−1.0214	0.18114	−0.0126	1.2	−0.71205	0.72261	0.52823	0.89509
0.2036	0.63806	0.47814	−0.29806	0.25911	5.6	−1.0736	0.22	−0.0119	1.2	−0.76497	0.71196	0.52348	0.8837
0.234	0.47035	0.54826	−0.30375	0.33535	5.6	−1.0617	0.20876	−0.0113	1.2	−0.80042	0.70239	0.5036	0.86427
0.309	0.21371	0.40219	−0.32518	0.21547	5.6	−1.1411	0.25033	−0.01	1.2	−0.78338	0.67763	0.51384	0.85042
0.3551	0.26445	0.53865	−0.12798	−0.059858	5.8	−1.1955	0.2752	−0.0092	1.2	−0.80564	0.67603	0.51955	0.85261
0.3896	0.22985	0.37837	−0.17963	−0.1794	6.0	−1.2198	0.28433	−0.0087	1.2	−0.80017	0.67721	0.52797	0.85869
0.4274	0.15141	0.38935	−0.16038	−0.23629	6.0	−1.2482	0.29598	−0.0082	1.2	−0.78776	0.67813	0.52869	0.85987
0.469	0.16058	0.50207	−0.12662	−0.19127	6.0	−1.2701	0.28918	−0.0076	1.2	−0.75596	0.6766	0.53087	0.86001
0.5913	0.002014	0.53098	−0.11966	−0.20467	6.0	−1.333	0.30084	−0.0062	1.2	−0.69906	0.67075	0.54401	0.86363
0.7456	−0.15653	0.72445	−0.034817	−0.21396	6.0	−1.3807	0.30533	−0.0049	1.2	−0.69977	0.66021	0.51272	0.83592
0.818	−0.16834	0.75771	−0.025654	−0.2371	6.0	−1.4197	0.31184	−0.0043	1.2	−0.67981	0.66009	0.50054	0.8284
0.9401	−0.29156	0.79742	−0.043022	−0.2024	6.0	−1.4362	0.30951	−0.0036	1.2	−0.66069	0.66081	0.47738	0.81521
1.3622	−0.80425	0.71213	−0.048474	−0.1361	6.0	−1.5354	0.34887	−0.002	1.2	−0.66646	0.64969	0.41806	0.77258

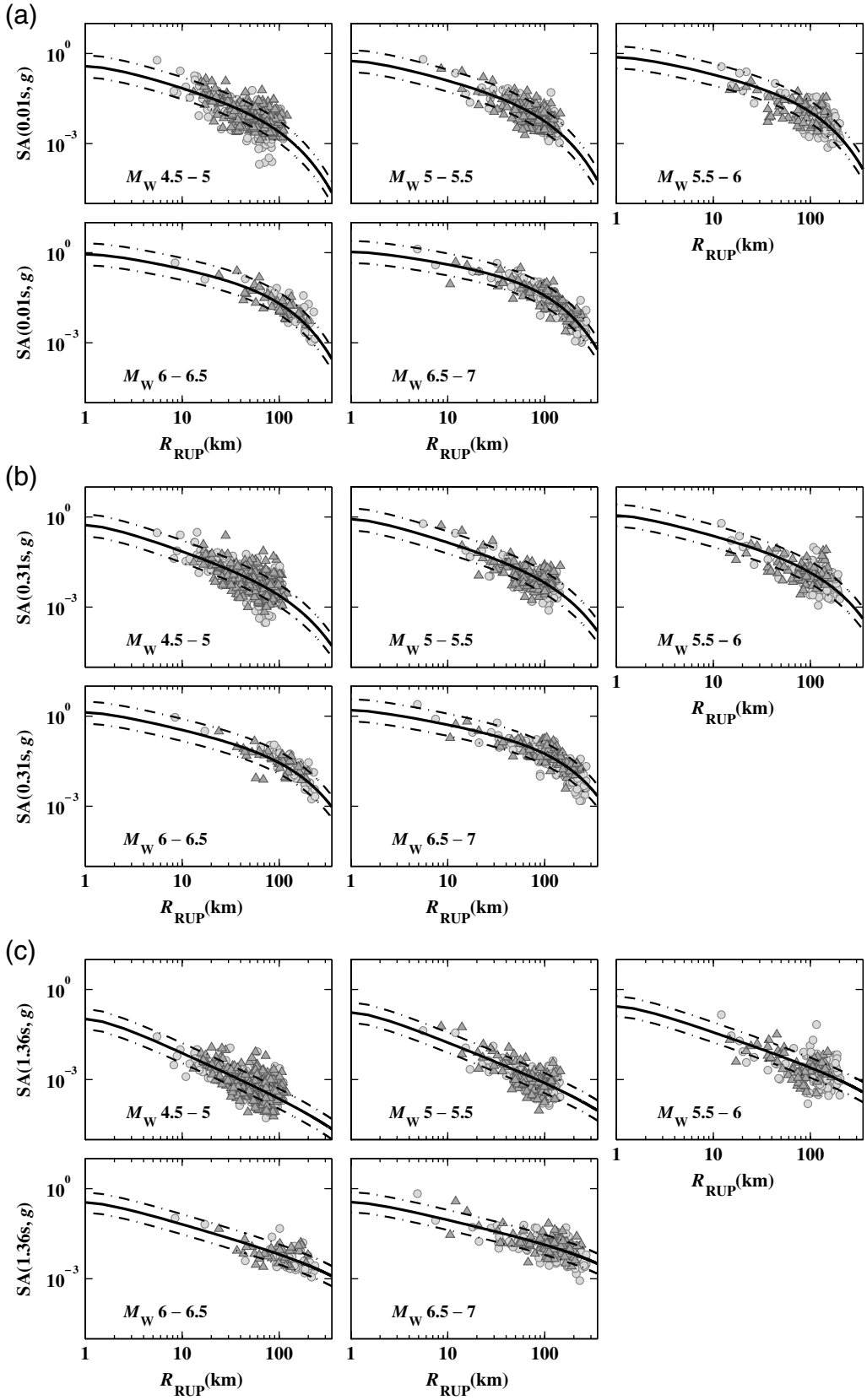

Figure 4. (a) Peak ground acceleration (PGA); spectral accelerations (SA) (b) (0.31 s) and (c) SA (1.36 s), as units of g, and differentiated according to the two networks (circles, KiK-net; triangles, K-NET networks), with respect to the predicted ground-motion attenuation model plotted as a function of R_{RUP} for the $500 \leq V_{S30} < 600$ m/s. The solid line in each subplot is the mean predicted model, and the dashed lines refer to ± 1 sigma.

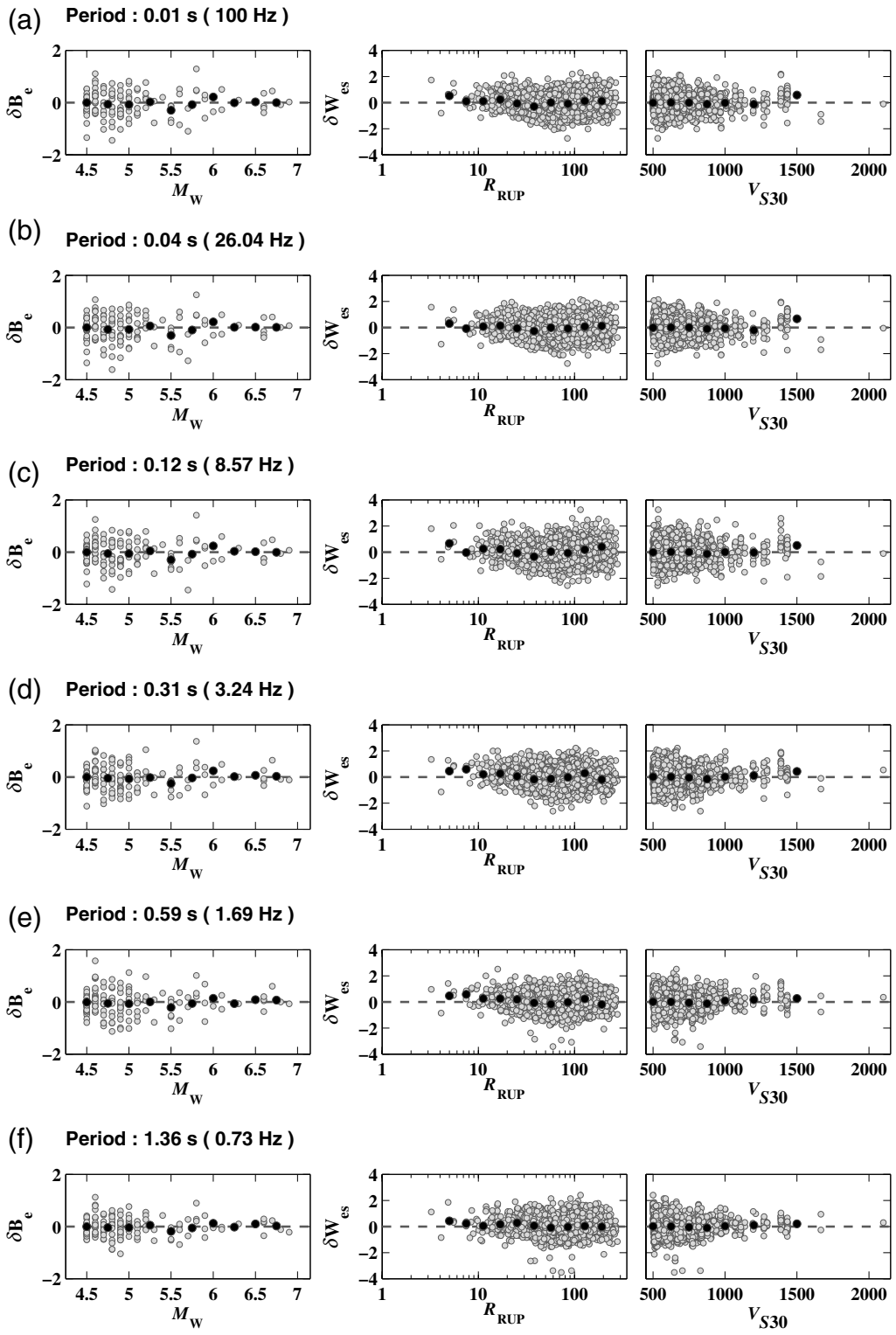

Figure 5. Interevent residuals plotted with respect to M_w and intraevent residuals as a function of R_{RUP} and V_{S30} for various spectral periods. The black dots represent the averages for a bin of M_w, R_{RUP}, or V_{S30}.

between soft rock and rock are obtained by computing ground motions using random vibrations (SMSIM program, Boore, 2003) with a magnitude of 6.0 at a distance of 20 km and with a site amplification function computed from the quarter-wavelength method and from generic profiles suggested by Boore and Joyner (1997) and extrapolated for various V_{S30} values by Cotton *et al.* (2006). The stochastic method input parameters are similar to those used by

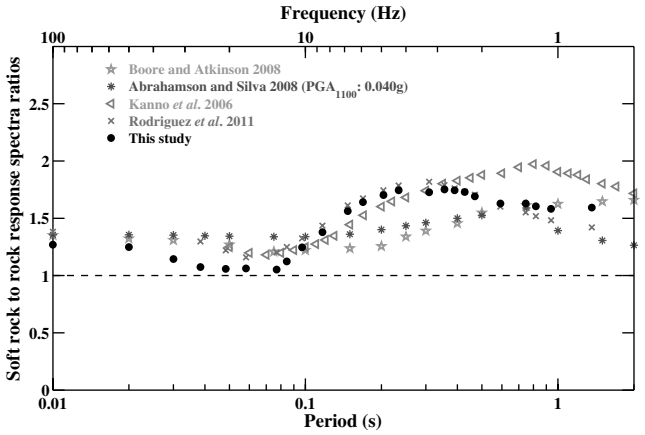

Figure 6. Soft-rock-to-rock empirical spectral amplification ratios (550/1100 m/s) estimated for the different GMPEs.

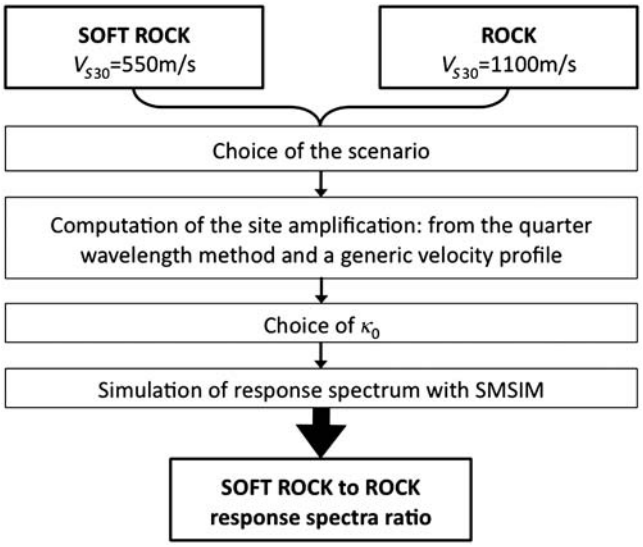

Figure 7. Flow chart of the methodology used for computing the soft-rock-to-rock response spectra ratios.

Campbell (2003) for western North America, except for the stress drop and the quality factor. For these parameters, we used the mean values given by Oth *et al.* (2010) and Oth, Bindi, *et al.* (2011): stress drop, 10 bars; quality factor, $Q(f) = 81 \times f^{0.71}$. Also, to simulate the characteristic responses of the instruments (Kinoshita, 1998), a three-pole Butterworth filter with a cutoff frequency of 30 Hz was added into the model (i.e., $f_{cut} = 30$ Hz and $n = 3$). The theoretical soft-rock-to-rock ratios were computed first for identical values of κ_0 and second for κ_0 values inferred from the V_{S30}. The V_{S30}–κ_0 relationships of Silva *et al.* (1998), Chandler *et al.* (2006), Edwards *et al.* (2011), and Van Houtte *et al.* (2011) were tested (see Fig. 8b).

Figure 8a shows the comparison of the theoretical ratios with the empirical ratio. First, the site term of the GMPE (see equation 5) is a function of V_{S30} only, and it might be expected that this empirical ratio follows the same trend as the theoretical ratios that are influenced only by V_{S30} (Fig. 8a, gray lines). The discrepancy between the empirical and the theoretical ratios computed with identical κ_0 value for the two rock sites indicates that the empirical site coefficient does not only take into account the V_{S30} effect. Second, the comparison between the empirical ratio and the theoretical ratios computed with two different κ_0 values for the two rock sites shows a similar general shape when the V_{S30}–κ_0 relationships of Silva *et al.* (1998), Chandler *et al.* (2006), and Van Houtte *et al.* (2011) are used, with a decrease from the PGA to 0.04–0.08 s and then an increase to 0.5 s (the step function). This comparison confirms the dependency of the rock-site responses on both κ_0 and V_{S30}, not on V_{S30} alone. However, none of the existing V_{S30}–κ_0 relationships does allow to fit perfectly the empirical ratio which indicates the need to improve these relationships or the velocity profiles used with the assumption of the quarter-wavelength approach in the stochastic modeling. For example, the observed amplification at periods larger than 1 s suggests impedance contrasts at depth not captured by the generic velocity profile.

Other parameters, like the scenario choice, might influence the shape of the theoretical ratios. Figure 9 shows this influence on the theoretical soft-rock-to-rock ratios considering the V_{S30}–κ_0 relationship of Van Houtte *et al.* (2011). Fluctuations are observed only at short periods, and especially for different distances. Variations in the amplification at different distances are related to the energy attenuation along the path. At large distances, the energy is largely dissipated, and so the κ_0 effect is less. In the same manner, the choice of the attenuation model affects the theoretical ratios. However, only consideration of some correlation between κ_0 and V_{S30} can reproduce the observed step function of the real data.

The shape of the empirical soft-rock-to-rock ratio is consistent with the theoretical rock-to-hard-rock ratio shape and confirm the interest of V_{S30}–κ_0 dependent stochastic simulations for host-to-target rock-site adjustments (Atkinson and Boore, 2011; Van Houtte *et al.*, 2011). The differences between theoretical and empirical functions confirm the need of a good calibration of κ_0 and *S*-wave velocity profiles to perfom these adjustments.

Toward New SA(f) Ground-Motion Prediction Equations that Include Site-Specific κ_0 Effects?

The comparison of the theoretical ratios with the empirical ratio showed that the site coefficient, which is dependent only on V_{S30}, takes into account a part of κ_0. This confirmed a correlation between κ_0 and V_{S30}. However, empirical coefficients that depend only on V_{S30} do not allow the full κ_0 effect to be taken into account single handedly. In the following section, we therefore seek to include both κ_0 and V_{S30} as parameters of GMPEs. It is thus necessary to have an estimate of κ_0 beforehand.

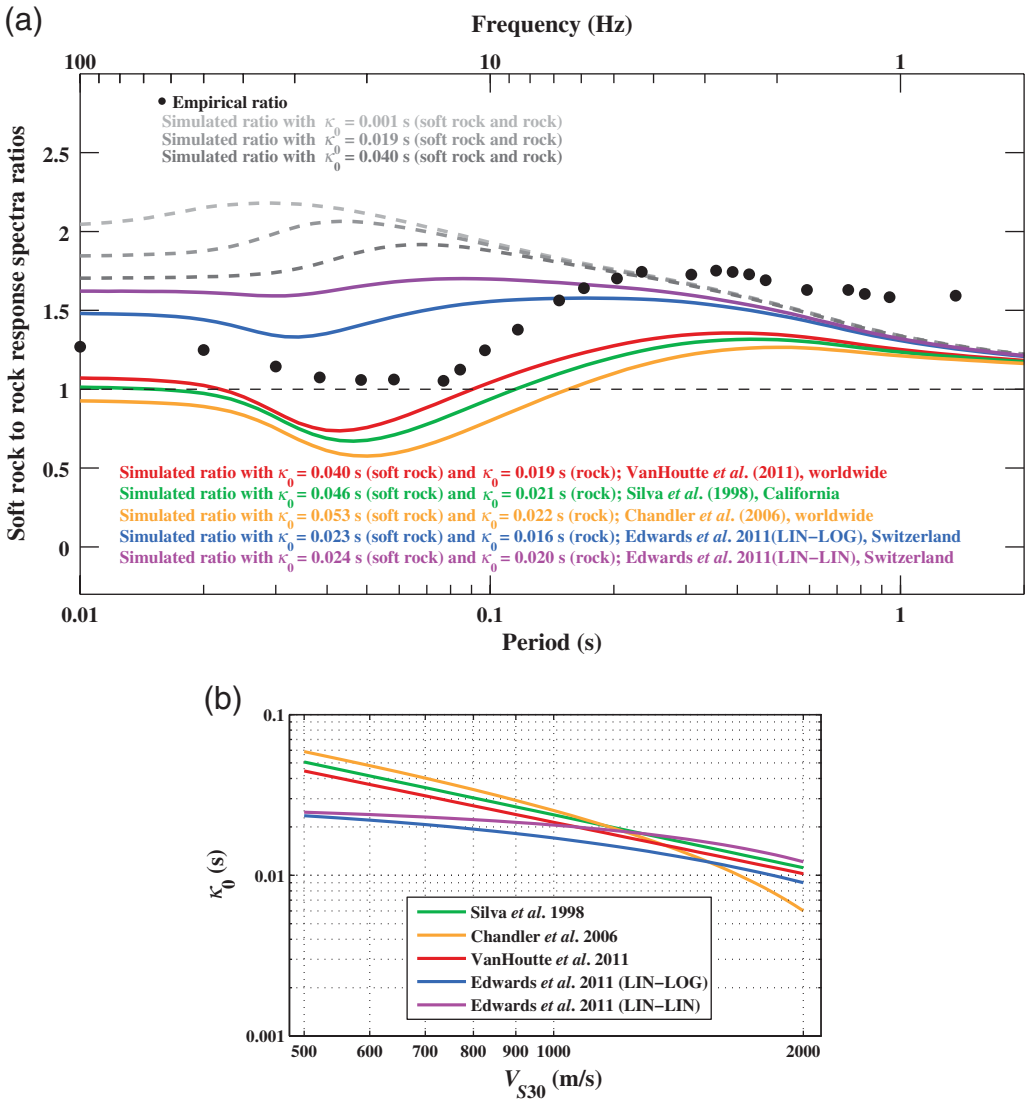

Figure 8. Intraevent residuals with respect to κ_{0_RESP1} at high frequencies: (a) when the empirical model of the 5% damped acceleration response spectra does not take into account κ_{0_RESP1} and (b) when it includes κ_{0_RESP1}.

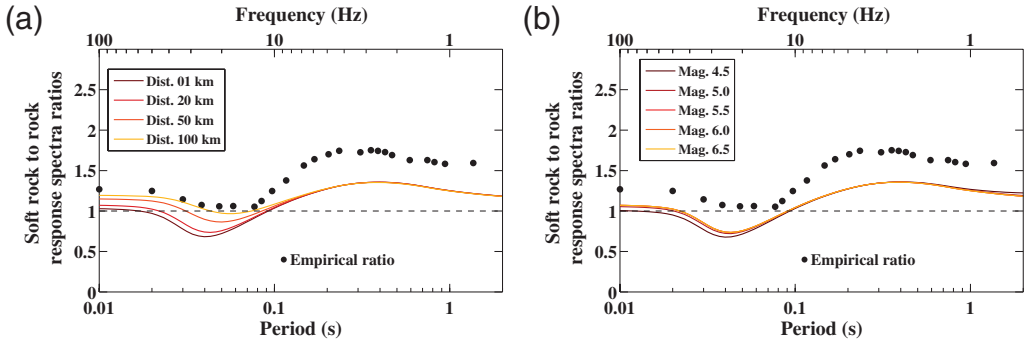

Figure 9. Soft-rock-to-rock spectral amplification ratios (550/1100 m/s) estimated using the site function coefficient from SA(f) GMPE (black dots) and the Boore (2003) stochastic method with κ_0 depending on V_{S30}, according to the Van Houtte *et al.* (2011) relationship (lines in shades of red) for different scenarios: (a) magnitude 6.0 and variation in the distance; (b) distance 20 km and variation in the magnitude.

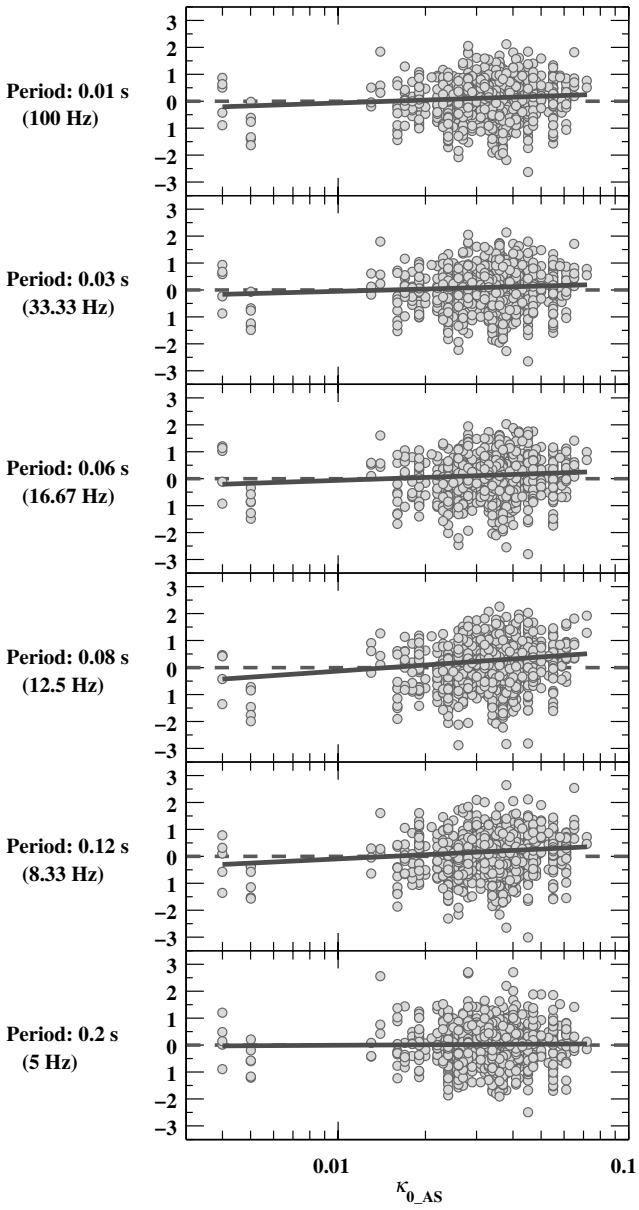

Figure 10. Intraevent residuals with respect to κ_{0_AS} at high frequencies when the empirical model of the 5% damped acceleration response spectra does not take κ_{0_AS} into account.

Van Houtte *et al.* (2011) assessed κ_0 on a Japanese dataset using the original method of Anderson and Hough (1984) (κ_{0_AS}). The intraevent residuals with respect to κ_{0_AS} are presented in Figure 10, for the frequency range corresponding to the measurement (between 5 and 50 Hz). The analysis of these residuals does not reveal any dependence of residuals with respect to κ_{0_AS}. Indeed, Van Houtte *et al.* (2011) assessed κ_{0_AS} without consideration of the response characteristic of the instrument that cuts the frequency content to 30 Hz. Accounting for the instrument response might be important; computing kappa for frequency ranges where the response is considered flat is one of the recommendations made by Ktenidou *et al.* (2013).

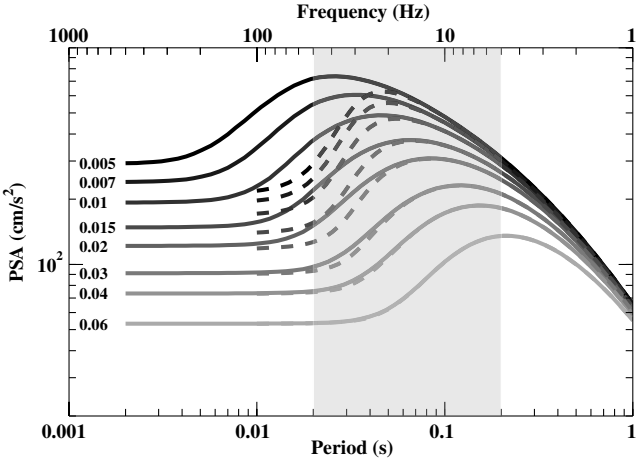

Figure 11. Illustration of the effect of the Japanese instrument response characteristic on the simulated response spectra computed with SMSIM program for different κ_0 values. Comparison of the unfiltered (solid lines) and filtered (dashed lines) acceleratation response spectra with magnitude 6.0, distance 20 km, V_{S30} = 800 m/s, stress drop = 80 bars, and sampling frequency of 100 Hz. The filter corresponds to a Butterworth filter with f_{cut} = 30 Hz and n = 3. The gray area corresponds to the frequency range of the κ_{0_AS} measurements of Van Houtte *et al.* (2011).

Figure 11 shows a comparison of the acceleration response spectra simulated for two cases, one including the low-pass filter and one without it, for a given scenario and for various κ_0 values. For high κ_0 values, the high-frequency part of the simulated response spectrum is strongly attenuated in the two cases. The κ_0 effect is significant across a wide range of frequency, from PGA to 1 s. The filter has a significant effect on the response spectra, particularly for the lower κ_0 value sites. For such sites, the method used by Van Houtte *et al.* (2011) will lead to overestimated κ_{0_AS} values. These considerations might explain the lack of trends observed with the κ_{0_AS} values of Van Houtte *et al.* (2011).

Given the frequency low-pass filter of the instrument and the large datasets, another more practical possibility to define the high-frequency attenuation in our case consists of fitting the observed response spectra (real data or GMPE) with simulations based on the stochastic model, in a similar way to Silva and Darragh (1995), Boore and Joyner (1997), Malagnini *et al.* (2000), and Biro and Renault (2012). This method is based on the fact that when the input parameter κ_0 of the simulations increases, the maximum and the plateau end of the simulated acceleration response spectra are shifted to lower frequencies. Thus, a relationship between the input parameter κ_0 and a selected parameter describing the acceleration response spectrum shape at high frequencies can be defined. Then, this new parameter, describing the high-frequency acceleration response spectral shape, is obtained from the observed response spectra and finally, the observed κ_0 is derived from the theoretical relationship. This new κ_0 obtained from theoretical response spectra is called κ_{0_RESP}, in accordance with the suggestions of Ktenidou *et al.* (2013).

Table 3
Definitions of the Different Frequencies Used to Characterize κ_0 from the Acceleration Response Spectra

$f_{amp}1$	Geometric mean of the two frequencies corresponding to 5% spectral acceleration below the peak of the acceleration response spectrum and on both sides of the peak spectral acceleration.
$f_{amp}2$	Highest frequency that corresponds to a spectral acceleration of double the peak ground acceleration.
$f_{amp}3$	Highest frequency that corresponds to a spectral acceleration of $\exp\left[\frac{\ln(SA_{peak})+\ln(PGA)}{2}\right]$.
$f_{amp}4$	Highest frequency that corresponds to a spectral acceleration of 1.5 times the peak ground acceleration.

Four frequency measures have been related to the input parameter κ_0 by L. Al Atik and N. Abrahamson (personal comm., 2012). These frequency definitions are given in Table 3. Figure 12a and 12b show these frequency measures on the simulated response spectra according to κ_0 in the unfiltered and filtered cases, respectively. When κ_0 decreases, all the f_{amp} measures appear to increase linearly in the unfiltered case, while the f_{amp} measures appear to increase faster for the lower κ_0 values in the filtered case, especially for the higher-frequency f_{amp} measures. In the following, these four frequency measures will be tested and κ_{0_RESP} will be assessed from the best parameter for the KiK-net and K-NET high V_{S30} sites.

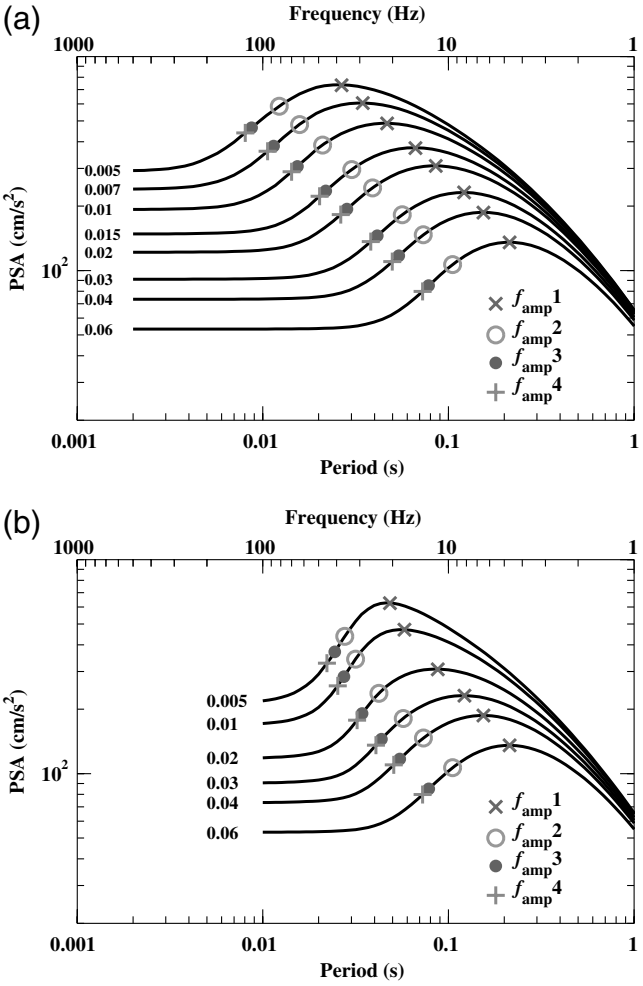

Figure 12. κ_0 effects on stochastic simulations of the 5% damped pseudoacceleration response spectrum, and the corresponding f_{amp} measures. The κ_0 values are indicated near to the corresponding spectrum. Simulated response spectra with magnitude 6.0, distance 20 km, V_{S30} = 800 m/s, stress drop = 80 bars, and sampling frequency of 100 Hz (a) without including the filter and (b) for the Japanese data (i.e., with a Butterworth filter with f_{cut} = 30 Hz and n = 3.)

Toward a Theoretical κ_0–f_{amp} Relationship Specific to the Japanese Dataset

Using the stochastic simulation method of Boore (2003) (the SMSIM program), we generated a large number of 5%-damped pseudoacceleration response spectra for different input parameters. These parameters are summarized in Table 4. The other input parameters of the model are similar of those used by Campbell (2003) for western North America.

First, the simulations were computed without and with the Japanese data filter mentioned in Kinoshita (1998), to examine the impact of this filter on the κ_0 measures. Figure 13 shows for each f_{amp} definition, the geometric mean of the resulting f_{amp} measures with respect to κ_0 in these two cases; that is, with a Butterworth filter with a cutoff frequency of 30 Hz, and without this filter (Fig. 13, black curves and light gray curves, respectively). It appears necessary to preserve the high-frequency content of the signal to develop κ_0–f_{amp} relationships, and so to assess low κ_{0_RESP} values. If the data are filtered, the κ_0–f_{amp} relationship must be defined on filtered simulations, because the filter has a strong impact on the spectral response at high frequencies, and thus on the determination of κ_0.

We then checked that the various f_{amp} measures were mainly controlled by κ_0, and not by the stress drop, quality factor, distances, moment magnitude, and V_{S30}. Figure 14 shows the variability part of the $f_{amp}1$ measures from κ_0 and from the other input parameters as an example. All four f_{amp} measures are mainly controlled by κ_0, and the variability from the other input parameters is four times lower.

Figure 15 also shows the geometric mean of the resulting f_{amp} measures with respect to κ_0 in the Japanese case, with the low-pass filter applied in the frequency domain. To compare the relationships obtained, the f_{amp} values were normalized to the same frequency value for κ_0 = 0.075 s. First, for the four f_{amp} measures, there is a linear relationship between $\ln(\kappa_0)$ and $\ln(f_{amp})$ for the higher κ_0 values. $f_{amp}1$ is the measure for which there is a linear relationship on the widest range of κ_0, that is, from 0.075 to 0.015 s. For the other measures, this linear relationship ends at κ_0 = 0.025 s for $f_{amp}2$, and at κ_0 = 0.03 s for $f_{amp}3$ and $f_{amp}4$. The present study is focused on the analysis of rock-and-stiff-soil-motion data; that is, data with relatively small κ_0 values, according to previous studies (e.g., Van Houtte *et al.*, 2011), and the κ_0–f_{amp} relationship

Table 4
Seismological Parameters Used in the Stochastic Models

Parameters	Tested Values	References
$\Delta\sigma$	1, 10, and 100 bars 200 bars	Oth *et al.* (2010)
$Q(f) = Q_0 \times f^N$	$Q_0 = 91$ and $N = 0.64$ $Q_0 = 127$ and $N = 0.61$ $Q_0 = 55$ and $N = 0.77$ $Q_0 = 51$ and $N = 0.82$	Oth *et al.* (2011b)
V_{S30}	500, 700, 900, 1100, 1300 m/s	Boore and Joyner (1997), Cotton *et al.* (2006)
κ_0	0.002, 0.003, 0.004, 0.005, 0.006, 0.007, 0.008, 0.009, 0.01, 0.015, 0.02, 0.025, 0.03, 0.035, 0.04, 0.045, 0.05, 0.055, 0.06, 0.065, 0.07, and 0.075 s.	
M_w	4.5, 5.0, 5.5, 6.0, and 6.5	
Distances	5, 10, 20, 30, 40, 50 km	
Filter	with a Butterworth filter ($f_{max} = 30$ Hz and $n = 3$) and without	Kinoshita (1998)

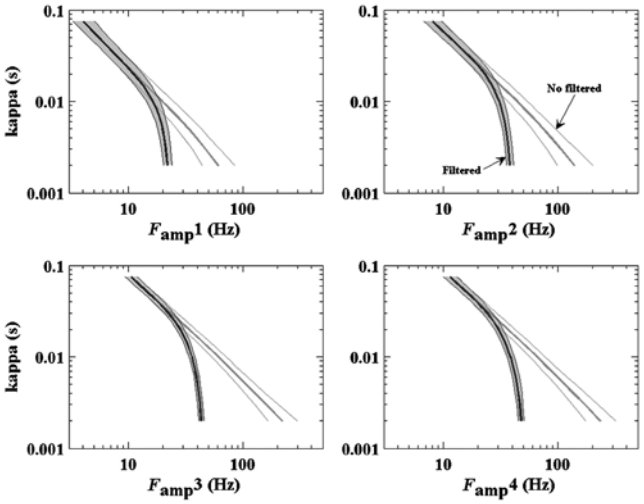

Figure 13. f_{amp} measurements with respect to the κ_0 values used to compute the 5% damped pseudoacceleration response spectra. The solid lines correspond to the geometric mean and the shading to the standard deviations (± 1 sigma). The parameters used to simulate the response spectra are summarized on Table 4. The sampling frequency was 100 Hz. The black curves correspond to simulations with a Butterworth filter ($f_{cut} = 30$ Hz and $n = 3$), and the light gray curves correspond to simulations without the filter.

should determine the low κ_{0_RESP} values for the hardest rocks. Therefore, $f_{amp}1$ is chosen to assess κ_{0_RESP1}. We define a linear relationship between $\ln(f_{amp}1)$ and $\ln(\kappa_0)$ for $f_{amp}1 \le 12$ Hz, and a logarithmic relationship for higher $f_{amp}1$. These relationships, which are valid only for Japan, $4.5 \le M_w \le 6.5$, $R_{RUP} \le 50$ km and $500 \le V_{S30} \le 1300$ m/s, are the following:

$$\ln(\kappa_0) = \begin{cases} -1.3224 \times \ln(f_{amp}1) - 0.73458 & \text{for } f_{amp}1 \le 12 \text{ Hz} \\ 0.84209 \times \ln[-\ln(f_{amp}1) + \ln(23)] - 3.65770 & \text{for } f_{amp}1 > 12 \text{ Hz} \end{cases} \quad (7)$$

This logarithmic relationship allows the effects of the frequency low-pass filter applied to the Japanese dataset to be taken into account. We limit this relationship to $\kappa_0 \ge 5$ ms (i.e., about $f_{amp}1 \le 20$ Hz).

Observed $f_{amp}1$ Measures for the Japanese Dataset

$f_{amp}1$ is computed on our Japanese high V_{S30} site dataset, on each record that validates the following criteria:

1. records with M_w greater than 4.5, to ensure that the source corner frequency is small enough to avoid any trade-off with the $f_{amp}1$ measures (the κ_0–$f_{amp}1$ relationship is developed between 3 and 20 Hz);
2. records with R_{RUP} less than 50 km to limit the distance dependence attenuation of the ground motion (in the Japanese case, the regional distance dependence of $\kappa(r)$ is low at distances less than 50 km; Van Houtte *et al.*, 2011);
3. events and sites with a minimum of three records, to constrain the $f_{amp}1$ values.

These $f_{amp}1$ measurements are then associated with the respective sites by computing the geometrical mean. Finally, 53 sites within the 405 sites of our initial dataset are associated with an $f_{amp}1$ measurement. The κ_{0_RESP1} values are

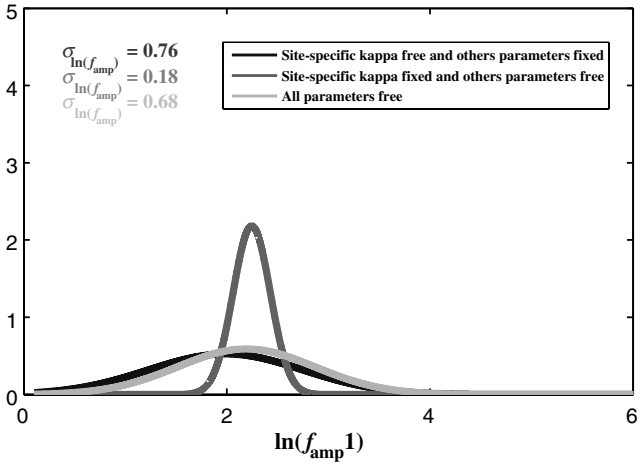

Figure 14. Analysis of the variability of $f_{amp}1$ measured from the simulated 5% damped pseudoacceleration response spectra.

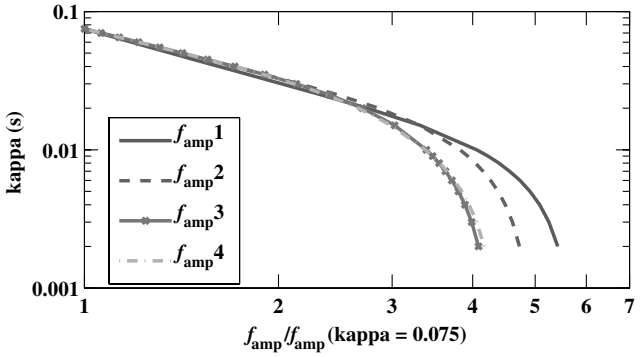

Figure 15. Normalized geometric mean of f_{amp} measurements with respect to the kappa values used to compute the 5% damped pseudoacceleration response spectra. The parameters used to simulate the response spectra are summarized on Table 4. The sampling frequency was 100 Hz, and a Butterworth filter was used with $f_{cut} = 30$ Hz and $n = 3$.

inferred from equation 7. Figure 16 shows the example of the $f_{amp}1$ computation for four sites. The *KMMH*11 site is the one with the highest V_{S30}, but not also with the highest $f_{amp}1$. Figure 17 shows the distribution of the κ_{0_RESP1} values. The geometrical mean of these measures is 0.023 s and the standard deviation is 0.51. This sigma value is slightly smaller than the one from the simulations ($\sigma_{\ln(f_{amp}1)} = 0.68$). Indeed, the difference might result from the limit of κ_0 values to values greater than 0.05 s or from an overestimation of the input parameter variability of the simulations.

Toward an Empirical SA(f) Model with κ_{0_RESP1}

Intraevent residuals show a clear trend with κ_{0_RESP1} (Fig. 18 left) and the model overestimates the observations with high κ_{0_RESP1} values. This overestimation is largest at 0.06 s, with a deviation from the mean of 1.3. Therefore, we chose to integrate the κ_{0_RESP1} effect within the site function up to 0.20 s. This period limit also corresponds to a frequency that is known as f_E, above which $\kappa(r)$ is usually measured on real data (Douglas *et al.*, 2010, reported f_E between 1 and 10 Hz). The new site function has the following functional form:

$$F_{S_j}(T) = c_1(T) \times \ln(V_{S30_j}/800) + c_2(T) \times \kappa_{0\_RESP1} \quad \text{for } T \leq 0.20 \text{ s}. \tag{8}$$

The a_1 and c_2 regression coefficients were calculated from the records for which $f_{amp}1$ was available: 701 records, 123 events, and 53 sites. The resulting coefficients are given in Table 5. Figure 19 shows for a given scenario the predicted response spectra for different κ_{0_RESP1} values. The κ_{0_RESP1} effect is significant with the new empirical model (factor 4). For a typical scenario of moderate seismicity regions

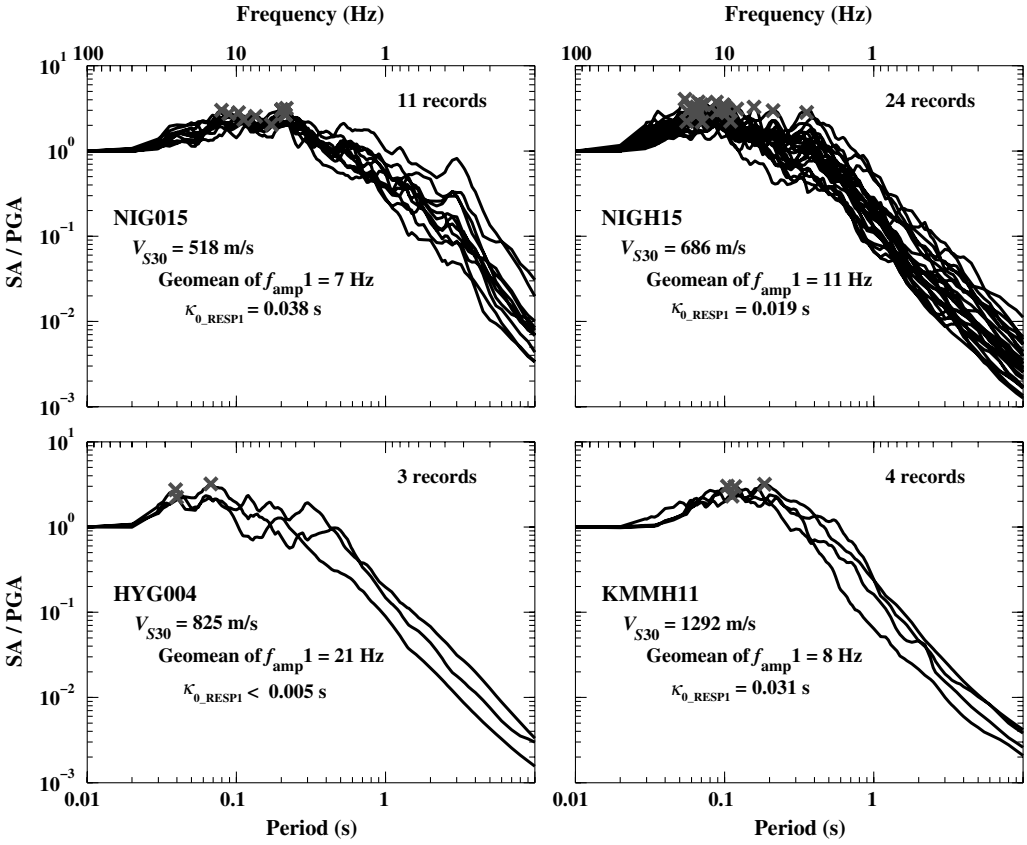

Figure 16. Examples of the $f_{amp}1$ computation on real data (i.e., geometric mean of the two horizontal components of the 5% damped acceleration response spectra). The crosses represent the $f_{amp}1$ for each spectrum.

Table 5
Regression Coefficients for the Predicted Model of the 5% Damped Acceleration Response Spectra (Geometrical Mean of the Two Horizontal Components, g), Including κ_{0_RESP1}

Period (s)	a_1	c_2	ϕ	τ	σ
0.01	0.42164	−18.3175	0.6194	0.54418	0.82449
0.02	0.47616	−19.2284	0.61694	0.54421	0.82267
0.03	0.84226	−22.4259	0.60808	0.55389	0.82253
0.0384	1.2858	−26.3715	0.60226	0.55729	0.82054
0.0484	1.6516	−30.0391	0.60972	0.56265	0.82966
0.0582	1.8443	−32.3928	0.62191	0.56861	0.84266
0.0769	1.9681	−31.5784	0.66571	0.56683	0.87434
0.0844	1.8935	−30.6174	0.68027	0.5576	0.87959
0.097	1.6602	−25.134	0.6852	0.55441	0.8814
0.1167	1.2164	−14.4499	0.69951	0.53759	0.88222
0.1472	0.87951	−5.1709	0.72769	0.55255	0.9137
0.1691	0.67908	−0.45114	0.70159	0.567	0.90206
0.2036	0.36475	2.7129	0.66326	0.56717	0.8727

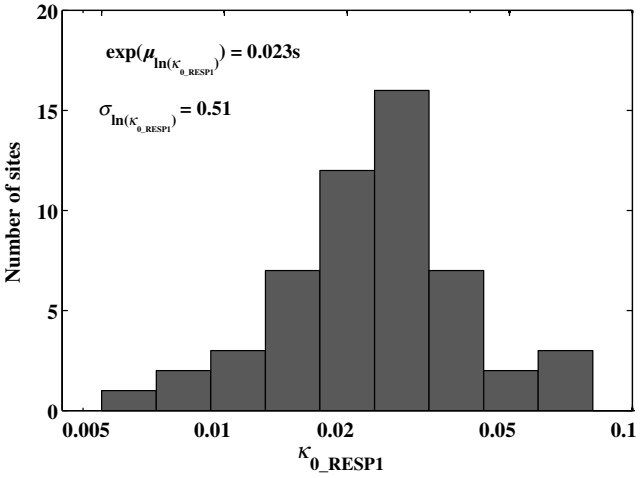

Figure 17. Distribution of the κ_{0_RESP1} values estimated for the 53 Japanese sites.

(M_w 6.0 and $R_{RUP} = 20$ km), the PGA variation is around 100 cm/s^2, between κ_{0_RESP1} of 0.005 s and κ_{0_RESP1} of 0.060 s. Here, the shift of the maximum spectral acceleration toward the low frequencies when κ_{0_RESP1} increases is significant.

Figure 18 (right) also shows the new intraevent residuals according to κ_{0_RESP1}. These residuals are well distributed and the intraevent variability is lower (Tables 2 and 5): at 0.06 s, the intraevent standard deviation goes from 0.71 to 0.62.

Conclusions

For seismic-hazard analysis, a standard rock definition is a key issue (e.g., as a basis for hazard or amplification computations). Site response is basically controlled by the velocity profile and rock damping characteristics. In most studies, however, rock motion is defined in relation to the single proxy parameter V_{S30}.

A new and homogeneous active shallow crustal accelerometric dataset of ground-motion records on high V_{S30} sites was built ($V_{S30} \geq 500$ m/s). This dataset consists of 2357 Japanese digital records. A new, rock- and stiff-soil-specific, SA(f) GMPE was derived using this new dataset. This new GMPE takes into account recent developments (analysis of both intravariability and intervariability, updated functional forms, including the scaling relations and V_{S30}). Our equation should be used only for predictor variables in these ranges: $4.5 \leq M_w \leq 6.9$; the limit of R_{RUP} is given by the Kanno *et al.* (2006) GMPE for a PGA threshold of 2.5 cm/s^2; and finally, $500 \leq V_{S30} \leq 1500$ m/s. The intraevent standard deviation is stronger than that derived in other regions, which confirms that the Japanese sites might be more heterogeneous than the European and Californian sites.

The empirical soft-rock-to-rock site function obtained has a step function, like for previous studies. The comparison with simulated site functions shows that the rock-site response is not only dependent on V_{S30}, but also takes into account part of κ_0. The empirical ratio form is roughly similar to the simulated ratio, incorporating a V_{S30}–κ_0 relationship with a strong dependency on the two parameters. This site coefficient analysis of the SA(f) confirms (1) the dependency of rock amplifications on both V_{S30} and κ_0 and (2) the need to take into account both of these parameters for rock-site adjustments.

The integration of the site-specific κ_0 effect in the empirical model appears essential to more accurately describe the rock-and-stiff-soil-site function. Indeed, the simulations show that κ_0 variations produce large ground-motion differences. The κ_{0_AS} estimates of Van Houtte *et al.* (2011) were biased by the frequency low-pass filter of the instrument, and along with the very large volume of data, which is why we used an alternative method to evaluate the site-specific κ_0. The stochastic ground-motion simulations show that the site-specific κ_0 controls the frequency corresponding to the maximum response spectral acceleration ($f_{amp}1$). Thus, we can use theoretical κ_0–$f_{amp}1$ relationships derived from simulations to define κ_{0_RESP1} for our data. Finally, we include κ_{0_RESP1} explicitly as a term in the GMPE for periods below 0.2 s, to improve the prediction of the spectral acceleration at high frequencies, and to reproduce large spectral amplitude variations due to κ_0 differences.

We believe that the explicit inclusion of the site-specific κ_0 in the formulation of future GMPEs will help responses at high frequencies to be better described. However, such an improvement is currently limited by the lack of a physical understanding of the origins of this parameter, by the lack of consensus of a robust measurement method and the fact that instrumentation characteritics may filter high-frequency motions on low kappa sites. The recommendations of Ktenidou *et al.* (2013), for instance, can lead to a more robust estimate of κ_0 in the original manner of Anderson and Hough (1984). Several studies have linked the site-specific κ_0 with V_{S30}, although these correlations showed large variability, and thus it is not recommended to use κ_0 from these correlations

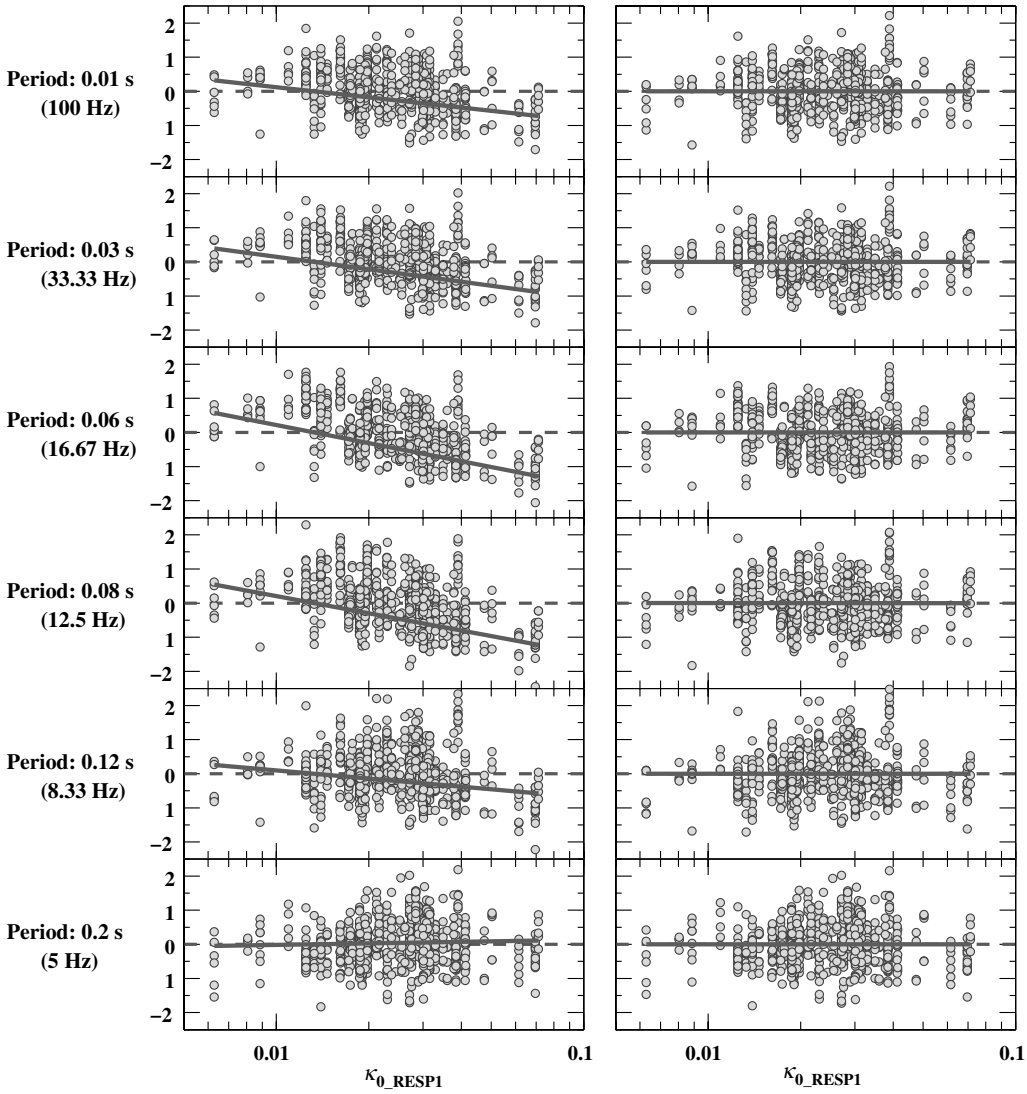

Figure 18. Intraevent residuals with respect to κ_{0_RESP1} at high frequencies: first, when the empirical model of the 5% damped acceleration response spectra does not take into account κ_{0_RESP1} (left), and, second, when it includes κ_{0_RESP1} (right).

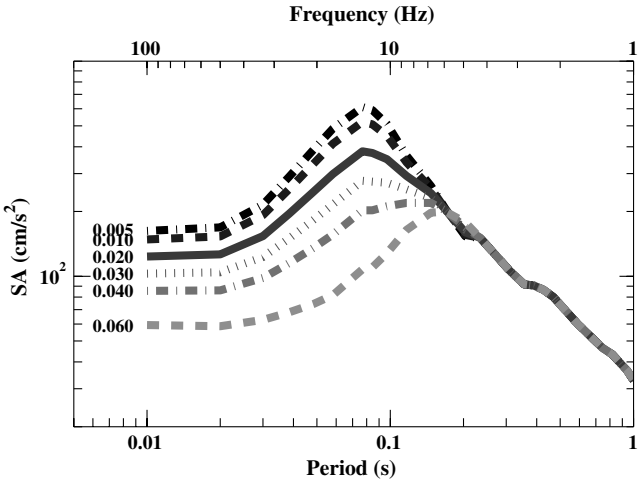

Figure 19. New 5% damped acceleration response spectra prediction model plotted for different κ_{0_RESP1} values, a magnitude of 6.0, a distance of 20 km, and a V_{S30} of 800 m/s.

(Ktenidou *et al.*, 2013). An alternative site-specific κ_0 estimate is proposed in the present study (κ_{0_RESP1}). However, enough records are needed to characterize it for the given rock site, and these need to come from short distances, to eliminate path effects and regional attenuation, and from large enough magnitudes, to ensure that source and corner frequency effects do not enter the computation.

Data and Resources

Accelerograms and geotechnical data from KiK-net and K-NET networks are available at http://www.k-net.bosai.go.jp (last accessed January 2012). The moment magnitude and hypocentral locations have been provided by the F-NET network at http://www.fnet.bosai.go.jp/freesia/top.php?LANG=en (last accessed January 2012). Figure 1 was made using Generic Mapping Tools v.3.4 (www.soest.hawaii.edu/gmt, last accessed August 2010; Wessel and

Smith, 1998). We used the SMSIM v.3.23 program package provided by Dave Boore (U.S. Geological Survey).

Acknowledgments

This research was supported by the French Atomic Agency (CEA) and the Institut Laue Langevin through the CASHIMA-SIGMA project. Discussions during the CASHIMA-SIGMA project and the Pegasos Refinement Project have been very useful and shaped some of the ideas developed in this paper. Specific thanks go to Norm Abrahamson, Linda Al Atik, Pierre-Yves Bard, Véronique Caillot, and Franck Scherbaum. We are indebted to the National Research Institute for Earth Science and Disaster Prevention (NIED), Japan, for providing the data for this analysis and to Hadi Ghasemi for providing the fault-plane models. We have benefited from the experience of Adrian Rodriguez, Gonzalo Montalva, Sinan Akkar, and Abdullah Sandikkaya regarding the regression procedure. We thank Adrien Oth and an anonymous reviewer for their critical reviews. Their comments and suggestions, together with those of Associate Editor H. Kawase, contributed appreciably to a major improvement of the article.

References

Abrahamson, N., and W. Silva (2008). Summary of the Abrahamson & Silva NGA ground-motion relations, *Earthq. Spectra* **24,** 67.

Abrahamson, N., and R. Youngs (1992). A stable algorithm for regression analyses using the random effects model, *Bull. Seismol. Soc. Am.* **82,** no. 1, 505.

Akkar, S., and J. Bommer (2010). Empirical equations for the prediction of PGA, PGV, and spectral accelerations in Europe, the Mediterranean region, and the Middle East, *Seismol. Res. Lett.* **81,** no. 2, 195.

Al Atik, L., N. Abrahamson, J. Bommer, F. Scherbaum, F. Cotton, and N. Kuehn (2010). The variability of ground-motion prediction models and its components, *Seismol. Res. Lett.* **81,** no. 5, 794.

Ambraseys, N. (1995). The prediction of earthquake peak ground acceleration in Europe, *Earthq. Eng. Struct. Dynam.* **24,** no. 4, 467–490.

Anderson, J., and S. Hough (1984). A model for the shape of the Fourier amplitude spectrum of acceleration at high frequencies, *Bull. Seismol. Soc. Am.* **74,** no. 5, 1969–1993.

Aoi, S., T. Kunugi, and H. Fujiwara (2004). Strong-motion seismograph network operated by NIED: K-NET and KiK-net, *J. Jpn. Assoc. Earthq. Eng.* **4,** no. 3, 65–74.

Atkinson, G., and D. Boore (2011). Modifications to existing ground-motion prediction equations in light of new data, *Bull. Seismol. Soc. Am.* **101,** no. 3, 1121.

Biro, Y., and P. Renault (2012). Importance and impact of host-to-target conversions for ground motion prediction equations in PSHA, in *Proc. of the 15th World Conference on Earthquake Engineering, 1855*, Lisbon, Portugal.

Boore, D. (2003). Simulation of ground motion using the stochastic method, *Pure Appl. Geophy.* **160,** no. 3, 635–676.

Boore, D., and G. Atkinson (2008). Ground-motion prediction equations for the average horizontal component of PGA, PGV, and 5%-damped PSA at spectral periods between 0.01 s and 10.0 s, *Earthq. Spectra* **24,** 99.

Boore, D., and W. Joyner (1997). Site amplifications for generic rock sites, *Bull. Seismol. Soc. Am.* **87,** no. 2, 327–341.

Boore, D., W. Joyner, and T. Fumal (1997). Equations for estimating horizontal response spectra and peak acceleration from western North American earthquakes: A summary of recent work, *Seismol. Res. Lett.* **68,** no. 1, 128–153.

Boore, D., E. Thompson, and H. Cadet (2011). Regional correlations of V_{S30} and velocities averaged over depths less than and greater than 30 meters, *Bull. Seismol. Soc. Am.* **101,** no. 6, 3046–3059.

Borcherdt, R. (1970). Effects of local geology on ground motion near San Francisco Bay, *Bull. Seismol. Soc. Am.* **60,** no. 1, 29–61.

Building Seismic Safety Council (2000). The 2000 NEHRP recommended provisions for new buildings and other structures: Part I (Provisions) and Part II (Commentary), *Tech. rep., FEMA 368/369*, Federal Emergency Management Agency, Washington, D.C.

Cadet, H., P.-Y. Bard, and A. Rodriguez-Marek (2010). Defining a standard rock site: Propositions based on the KiK-net database, *Bull. Seismol. Soc. Am.* **100,** no. 1, 172–195.

Campbell, K. (2003). Prediction of strong ground motion using the hybrid empirical method and its use in the development of ground-motion (attenuation) relations in eastern North America, *Bull. Seismol. Soc. Am.* **93,** no. 3, 1012–1033.

Chandler, A., N. Lam, and H. Tsang (2006). Near-surface attenuation modelling based on rock shear-wave velocity profile, *Soil Dynam. Earthq. Eng.* **26,** no. 11, 1004–1014.

Chiou, B., R. Darragh, N. Gregor, and W. Silva (2008). NGA project strong-motion database, *Earthq. Spectra* **24,** 23.

Cotton, F., F. Scherbaum, J. Bommer, and H. Bungum (2006). Criteria for selecting and adjusting ground-motion models for specific target regions: Application to central Europe and rock sites, *J. Seismol.* **10,** no. 2, 137–156.

Delavaud, E., F. Cotton, S. Akkar, F. Scherbaum, L. Danciu, C. Beauval, S. Drouet, J. Douglas, R. Basili, M. A. Sandikkaya, M. Segou, E. Faccioli, and N. Theodoulidis (2012). Toward a ground-motion logic tree for probabilistic seismic hazard assessment in Europe, *J. Seismol.* 1–23.

Douglas, J., P. Gehl, L. Bonilla, and C. Gélis (2010). A κ model for mainland France, *Pure Appl. Geophys.* **167,** no. 11, 1303–1315.

Edwards, B., D. Fäh, and D. Giardini (2011). Attenuation of seismic shear wave energy in Switzerland, *Geophys. J. Int.* **185,** 967–984.

European Committee for Standardization (CEN) (2004). Eurocode 8: Design of structures for earthquake resistance, part 1: General rules, seismic actions and rules for buildings., *Tech. Rept. EN 1998-1*, http://www.cen.eu/cenorm/homepage.htm (last accessed August 2008).

Fujiwara, H., S. Aoi, T. Kunugi, and S. Adachi (2004). Strong-motion observation networks of NIED: K-NET and KiK-net, http://www.cosmos-eq.org/events/wkshop_records_processing/papers/Fujiwara_paper.pdf (last accessed September 2013).

Fukushima, Y. (1997). Comment on ground motion attenuation relations for subduction zones, *Seismol. Res. Lett.* **68,** no. 6, 947–949.

Fukushima, Y., and T. Tanaka (1990). A new attenuation relation for peak horizontal acceleration of strong earthquake ground motion in Japan, *Bull. Seismol. Soc. Am.* **80,** no. 4, 757–783.

Hanks, T. C. (1982). $f_{\max}$, *Bull. Seismol. Soc. Am.* **72,** 1867–1879.

Hikima, K., and K. Koketsu (2005). Rupture processes of the 2004 Chuetsu (mid-Niigata prefecture) earthquake, Japan: A series of events in a complex fault system, *Geophys. Res. Lett.* **32,** no. 18, L18303, doi: 10.1029/2005GL023588.

Horikawa, H. (2001). Earthquake doublet in Kagoshima, Japan: Rupture of asperities in a stress shadow, *Bull. Seismol. Soc. Am.* **91,** no. 1, 112.

Ide, S. (1999). Source process of the 1997 Yamaguchi, Japan, earthquake analyzed in different frequency bands, *Geophys. Res. Lett.* **26,** no. 13, 1973–1976.

Ikeda, T., K. Kamae, S. Miwa, and K. Irikura (2002). Source characterization and strong ground motion simulation of the 2000 tottori-ken seibu earthquake using the empirical green's function method, *J. Struct. Constr. Eng.* **561,** 37–45.

Japan Road Association (1980). Specifications for highway bridges, *Part V, Seismic Design*, Maruzen Co., LTD.

Japan Road Association (1990). Specifications for highway bridges, *Part V, Seismic Design*, Maruzen Co., LTD.

Kanno, T., A. Narita, N. Morikawa, H. Fujiwara, and Y. Fukushima (2006). A new attenuation relation for strong ground motion in Japan based on recorded data, *Bull. Seismol. Soc. Am.* **96,** no. 3, 879.

Kinoshita, S. (1998). Kyoshin net (K-NET), *Seismol. Res. Lett.* **69,** no. 4, 309–332.

Kobayashi, R., S. Miyazaki, and K. Koketsu (2006). Source processes of the 2005 West Off Fukuoka Prefecture earthquake and its largest aftershock inferred from strong motion and 1-Hz GPS data, *Earth Planets Space* **58,** no. 1, 57–62.

Ktenidou, O.-J., F. Cotton, N. Abrahamson, and J. Anderson (2013). Taxonomy of kappa: A review of definitions and estimation approaches targeted to applications, *Seismol. Res. Lett.* **85,** no. 1, doi: 10.1785/0220130027.

Ktenidou, O.-J., C. Gélis, and L.-F. Bonilla (2013). A study on the variability of kappa (κ) in a borehole: Implications of the computation process, *Bull. Seismol. Soc. Am.* **103,** no. 2A, 1048–1068.

Maeda, T., and T. Sasatani (2009). Strong ground motions from an M_j 6.1 inland crustal earthquake in Hokkaido, Japan: The 2004 Rumoi earthquake, *Earth Planets Space* **61,** no. 6, 689–701.

Malagnini, L., R. Herrmann, and M. Di Bona (2000). Ground-motion scaling in the Apennines (Italy), *Bull. Seismol. Soc. Am.* **90,** no. 4, 1062–1081.

Miura, S., Y. Suwa, T. Sato, K. Tachibana, and A. Hasegawa (2004). Slip distribution of the 2003 northern Miyagi earthquake (M 6. 4) deduced from geodetic inversion, *Earth Planets Space* **56,** no. 2, 95–101.

Miyake, H., K. Koketsu, K. Hikima, M. Shinohara, and T. Kanazawa (2010). Source fault of the 2007 Chuetsu-oki, Japan, earthquake, *Bull. Seismol. Soc. Am.* **100,** no. 1, 384.

Momiyama, S., K. Hikima, and K. Koketsu (2009). Joint inversion for the source process of the 2007 Noto Hanto earthquake with improved velocity structure models, in *Abstr. Jpn. Geosci. Union Meet. 2009*, S148–P006 (CD–ROM).

Nakahara, H., T. Nishimura, H. Sato, M. Ohtake, S. Kinoshita, and H. Hamaguchi (2002). Broadband source process of the 1998 Iwate prefecture, Japan, earthquake as revealed from inversion analyses of seismic waveforms and envelopes, *Bull. Seismol. Soc. Am.* **92,** no. 5, 1708.

Okada, Y., K. Kasahara, S. Hori, K. Obara, S. Sekiguchi, H. Fujiwara, and A. Yamamoto (2004). Recent progress of seismic observation networks in Japan-Hi-net, F-net, K-NET and KiK-net, *Earth Planets Space* **56,** xv–xxviii.

Oth, A., D. Bindi, S. Parolai, and D. Di Giacomo (2010). Earthquake scaling characteristics and the scale-(in) dependence of seismic energy-to-moment ratio: Insights from KiK-net data in Japan, *Geophy. Res. Lett.* **37,** L19304, doi: 10.1029/2010GL044572.

Oth, A., D. Bindi, S. Parolai, and D. Di Giacomo (2011). Spectral analysis of K-NET and KiK-net data in Japan, Part II: On attenuation characteristics, source spectra, and site response of borehole and surface stations, *Bull. Seismol. Soc. Am.* **101,** no. 2, 667.

Oth, A., S. Parolai, and D. Bindi (2011). Spectral analysis of K-NET and KiK-net data in Japan, Part I: Database compilation and peculiarities, *Bull. Seismol. Soc. Am.* **101,** no. 2, 652–666.

Regnier, J., A. Laurendeau, A. Duval, and P. Gueguen (2010). From heterogeneous set of soil data to V_S profile application on the French permanent accelerometric network (RAP) sites, in *Proc. 14EECE Ohrid, Macedonia Republic*, 30 August–3 September.

Rodriguez-Marek, A., G. Montalva, F. Cotton, and F. Bonilla (2011). Analysis of single-station standard deviation using the KiK-net data, *Bull. Seismol. Soc. Am.* **101,** no. 3, 1242.

Silva, W., and R. Darragh (1995). Engineering characterization of earthquake strong ground motion recorded at rock sites, Electric Power Research Institute, *Report TR-102261*, Palo Alto, California.

Silva, W. J., I. G. Wong, and R. B. Darragh (1995). Engineering characterization of earthquake strong ground motions in the Pacific Northwest, in *Assessing Earthquake Hazards and Reducing Risk in the Pacific Northwest*, *U.S. Geol. Surv. Profess. Pap. 1560*.

Van Houtte, C., S. Drouet, and F. Cotton (2011). Analysis of the origins of κ (Kappa) to compute hard rock to rock adjustment factors for GMPEs, *Bull. Seismol. Soc. Am.* **101,** no. 6, 2926–2941.

Wessel, P., and W. H. F. Smith (1998). New, improved version of the generic mapping tools released, *Eos Trans. AGU* **79,** 579 pp.

Yenier, E., M. Sandikkaya, and S. Akkar (2010). Report on the fundamental features of the extended strong groundmotion databank prepared for the SHARE project, *Deliverable 4.1 of Seventh Framework Programme Project Seismic Hazard Harmonization in Europe*, SHARE.

Yokota, Y., K. Koketsu, K. Hikima, and S. Miyazaki (2009). Ability of 1-Hz GPS data to infer the source process of a medium-sized earthquake: The case of the 2008 Iwate-Miyagi Nairiku, Japan, earthquake, *Geophys. Res. Lett.* **36,** no. 12, L12301, doi: 10.1029/2009GL037799.

Zhao, J., K. Irikura, J. Zhang, Y. Fukushima, P. Somerville, A. Asano, Y. Ohno, T. Oouchi, T. Takahashi, and H. Ogawa (2006). An empirical site-classification method for strong-motion stations in Japan using H/V response spectral ratio, *Bull. Seismol. Soc. Am.* **96,** no. 3, 914–925.

ISTerre, CNRS
Université Joseph Fourier
BP 53, 38041 Grenoble Cedex 9
France
aurore.laurendeau@ujf-grenoble.fr
fabrice.cotton@ujf-grenoble.fr
olga.ktenidou@ujf-grenoble.fr
(A.L., F.C., O.-J.K.)

Université Paris-est–IFSTTAR
Laboratoire Séismes et Vibrations
14-20 boulevard Newton
Cité Descartes, Champs sur Marne
F-77447 Marne-La-Vallée Cedex 2
France
luis-fabian.bonilla-hidalgo@ifsttar.fr
(L.-F.B.)

CEA
CEA Cadarache
13108 St Paul lez Durance Cedex
France
fabrice.hollender@cea.fr
(F.H.)

Manuscript received 24 January 2013;
Published Online 12 November 2013